

# THE RELATIVE ABUNDANCE OF COMPACT AND NORMAL MASSIVE EARLY-TYPE GALAXIES AND ITS EVOLUTION FROM REDSHIFT $Z \sim 2$ TO THE PRESENT.<sup>1</sup>

P. CASSATA<sup>2</sup>, M. GIAVALISCO<sup>2</sup>, YICHENG GUO<sup>2</sup>, A. RENZINI<sup>3</sup>, H. FERGUSON<sup>4</sup>, A. M. KOEKEMOER<sup>4</sup>, S. SALIMBENI<sup>2</sup>, C. SCARLATA<sup>5</sup>, N. A. GROGIN<sup>4</sup>, C. J. CONSELICE<sup>6</sup>, T. DAHLEN<sup>4</sup>, J. M. LOTZ<sup>4</sup>, M. DICKINSON<sup>7</sup>, AND LIHWAI LIN<sup>8</sup>

*Draft version November 22, 2018*

## ABSTRACT

We report on the evolution of the number density and size of early-type galaxies from  $z \sim 2$  to  $z \sim 0$ . We select a sample of 563 massive ( $M > 10^{10} M_{\odot}$ ), passively evolving ( $SSFR < 10^{-2} \text{Gyr}^{-1}$ ) and morphologically spheroidal galaxies at  $0 < z < 2.5$ , using the panchromatic photometry and spectroscopic redshifts available in the GOODS fields. We combine ACS and WFC3 HST images to study the morphology of our galaxies in their optical rest-frame in the whole  $0 < z < 2.5$  range. We find that throughout the explored redshift range the passive galaxies selected with our criteria have weak morphological K-correction, with size being slightly smaller in the optical than in the UV rest-frame (by  $\sim 20\%$  and  $\sim 10\%$  at  $z > 1.2$  and  $z < 1.2$ , respectively). We measure a significant evolution of the mass-size relation of early-type galaxies, with the fractional increment that is almost independent on the stellar mass. Early-type galaxies (ETGs) formed at  $z > 1$  appear to be preferentially small, and the evolution of the mass-size relation at  $z < 1$  is driven by both the continuous size growth of the compact galaxies and the appearance of new ETGs with large sizes. We also find that the number density of all passive early-type galaxies increases rapidly, by a factor of 5, from  $z \sim 2$  to  $z \sim 1$ , and then more mildly by another factor of 1.5 from  $z \sim 1$  to  $z \sim 0$ . We interpret these results as the evidence that the bulk of the ETGs are formed at  $1 < z < 3$  through a mechanism that leaves very compact remnants. At  $z < 1$  the compact ETGs grow gradually in size, becoming normal size galaxies, and at the same time new ETGs with normal-large sizes are formed.

*Subject headings:* cosmology: observations — galaxies: fundamental parameters — galaxies: evolution

## 1. INTRODUCTION

The epoch between  $z \sim 3$  and  $z \sim 1$  appears to be crucial for the assembly of massive galaxies, as many authors find that the number density of galaxies with masses around  $10^{11} M_{\odot}$  and larger evolves very rapidly over this period of time (Fontana et al. 2006; Marchesini et al. 2009; Ilbert et al. 2010; Conselice et al. 2011). By redshift  $z \sim 1$ , however, the number density of early-types is comparable to the local one, with an increase of a factor of 1.5 allowed at the most (Cimatti et al. 2006; Franceschini et al. 2006; Borch et al. 2006). There is also evidence that a substantial fraction of the massive elliptical galaxies at  $z > 1.5$  are smaller than their local counterparts of the same mass (Daddi et al. 2005; Trujillo et al. 2007; Toft et al. 2007; Zirm et al. 2007; Van Dokkum et al. 2008; Buitrago et al. 2008; Cimatti et al. 2008), whereas some passively evolving galaxies may be already present at redshifts as high as  $\sim 3$  (Van Dokkum et al. 2010; Guo et al. 2011a in prep.).

We still lack a comprehensive understanding of the formation of passively evolving galaxies and of their evolution in size and spatial abundance from  $z \sim 3$  to the present, including the physical mechanisms responsible for the quenching of star formation. Classically, hierarchical models of galaxy formation predict that the evolution of massive galaxies at early epochs is mostly driven by major mergers (e.g. Shankar et al. 2010, 2011) and that some form of feedback, from star formation itself or from AGN activity, quenches star formation (e.g. Somerville et al. 2008). But highly turbulent disks with  $SFR \sim 100 M_{\odot} \text{yr}^{-1}$  have been claimed to also be efficient into slowing accreting gas in recent works (Förster-Schreiber et al. 2006; Förster-Schreiber et al. 2009; Genzel et al. 2008). Others have suggested that at later epochs ( $z < 1$ ), the evolution is dominated by less violent processes, like minor mergers and/or smooth accretion (Van Dokkum et al. 2010), that can possibly explain the size evolution as well (Hopkins et al. 2009). Recently, Peng et al. (2010) have shown that two independent processes are responsible for the quenching, one related to mass (or almost equivalently to the star formation rate), and another to the environment via the local overdensity, with the former dominating especially at high masses and early cosmic times, whereas the latter dominates at low masses and late times.

Observationally, there is still ongoing debate on the quantitative and qualitative features of the evolution of early-type galaxies. For example, the detection of compact size, and thus large stellar density, is mostly based on morphological studies done either using *HST*/ACS  $z$ -band images, which at  $1 < z < 2$  sample the rest-

<sup>1</sup> Based on data obtained with the *Hubble Space Telescope* operated by AURA, Inc. for NASA under contract NAS5-26555.

<sup>2</sup> Department of Astronomy, University of Massachusetts, Amherst, MA 01003; paolo@astro.umass.edu

<sup>3</sup> Osservatorio Astronomico di Padova (INAF-OAPD), Vicolo dell'Osservatorio 5, I-35122, Padova Italy

<sup>4</sup> Space Telescope Science Institute, 3700 San Martin Boulevard, Baltimore, MD, 21218

<sup>5</sup> School of Physics and Astronomy, University of Minnesota, 116 Church Street S.E., Minneapolis, MN 55455

<sup>6</sup> University of Nottingham, School of Physics and Astronomy, Nottingham NG7 2RD

<sup>7</sup> NAO-Tucson, 950 North Cherry Avenue, Tucson, AZ 85719

<sup>8</sup> Institute of Astronomy & Astrophysics, Academia Sinica, Taipei 106, Taiwan

frame UV and thus might not reflect the morphology of the bulk of the stellar mass (Daddi et al. 2005; Trujillo et al. 2007; Cimatti et al. 2008); or on *HST*/NICMOS or ground-based near-IR images, which have substantially worse resolution and/or image quality than ACS, and thus are potentially affected by systematic errors (Toft et al. 2007; Zirm et al. 2007; Van Dokkum et al. 2008; Buitrago et al. 2008). Even when taking advantage of modern, high-quality near-IR imagers such as *HST*/WFC3, only quite small samples have been studied so far (Cassata et al. 2010; Szomoru et al. 2010).

One essential step to map the evolution of passively evolving galaxies is the measure of the distribution function of their size at various cosmic epochs. While such distribution function has been studied in the local universe, at  $z \sim 2$  the measures remain uncertain. There is evidence that the size of high-redshift early-type galaxies (ETG) covers a range that overlaps with those in the present-day universe (e.g. Saracco et al. 2010), whereas selection effects might contribute to underestimate the contribution by more extended galaxies in the high- $z$  samples (Mancini et al. 2010). In any case, the mass-size relation of passively evolving galaxies and its evolution with redshift still remains poorly constrained. Even at  $z \sim 0$ , the distribution function of the effective radius of early-type galaxies is not well characterized at the small end, with some groups suggesting that a compact population of early-types could be hidden among unresolved red objects (Shih & Stockton (2011)). Moreover, Valentiniuzzi et al. (2010a; 2010b) reported evidence of a rich population of compact passive galaxies at  $z \sim 0.04$  and  $z \sim 0.7$ , and Saracco et al. (2010) pointed out that the number density of  $z \sim 2$  compact galaxies is comparable with the local density of similarly small early-types.

Recently, various groups have analyzed the morphology of massive early-type galaxies at  $z \sim 2$  using WFC3 images in the HUDF and/or ERS field (both located within the boundaries of GOODS-South) and found that the size of passive galaxies at  $z \sim 2$  is almost independent of the wavelength, confirming previous results on the compactness of such galaxies (e.g., Cassata et al. 2010; Ryan et al. 2011; Szomoru et al. 2010). If indeed the rest-frame UV morphology of these galaxies is similar to that at optical wavelength this allows us to use the wider ACS database for statistically significant studies of the distribution function of their effective radius, its dependence with the stellar mass, and its evolution with redshift.

The aim of this paper is to compare the size distribution *in the same rest-frame optical* for homogeneous samples of early-type galaxies at  $0 < z < 2.5$ , selected in a consistent way, and to constrain the number evolution of normal and compact early-types over the same epoch. In particular, we exploit the GOODS multi-band dataset to build a robust sample of passive early-type galaxies at  $1.2 < z < 2.5$ , and a similar sample of galaxies at  $0 < z < 1.2$ . We complement those two with a sample of local early-type galaxies from the SDSS survey, selected using the same criteria. Using the SDSS sample, we establish the local mass-size relation, and we identify local compact ETGs. Classically, authors in literature consider compact any galaxies  $1 - \sigma$  below the local SDSS relation (Valentinuzzi et al. 2010a, Valentin-

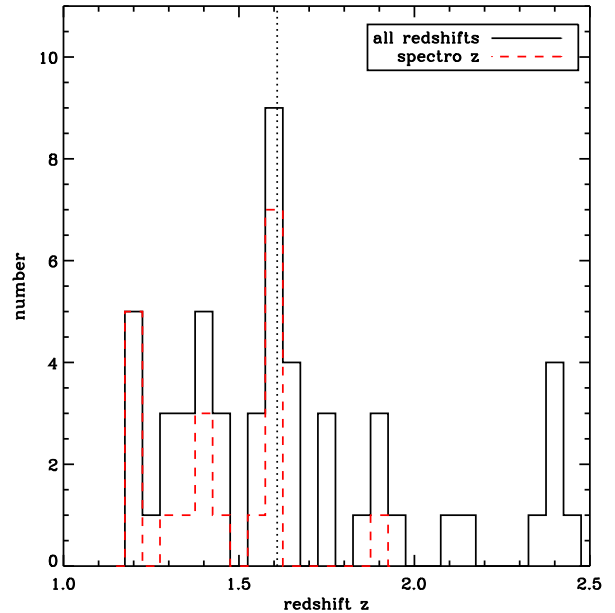


FIG. 1.— Redshift distribution in the highest redshift bin  $1.2 < z < 2.5$ . The continuous black line and the dashed one indicates all objects and objects with spectroscopic redshift, respectively. The vertical dotted line at  $z \sim 1.6$  indicates the median of the redshift distribution (that does not change considering spectroscopic objects only).

uzzi et al. 2010b, Saracco et al. 2010). This definition of compactness implies that 16% of the local galaxies are *compact*. In this paper, we use this definition, but we identify as well a class of *ultra-compact* early-type (at all redshifts) with size 0.4 dex below the local average relation. Virtually, there are no such dense galaxies in the local Universe. With the aim of constraining the evolutionary path that early-type galaxies follow from  $z \sim 2$  to the present, we compute the mass-density in *normal*, *compact* and *ultra-compact* early-types at  $0 < z < 2.5$ .

The issue that we try to clarify in this study is to which extent the evolution with cosmic time of the average mass-size relation is driven by the size growth of individual galaxies or by the progressive appearance of ETGs with larger size, as suggested by Valentinuzzi et al. (2010b).

Throughout the paper, we use a standard  $\Lambda$ CDM cosmology, with  $\Omega_\Lambda=0.7$ ,  $\Omega_M=0.3$  and  $H_0 = 70 \text{ Km s}^{-1} \text{ Mpc}^{-1}$ , and we assume a Salpeter IMF (Salpeter 1955).

## 2. DATA AND SAMPLE SELECTION

The GOODS-North and GOODS-South, centered on the Hubble Deep Field North (HDFN) and the Chandra Deep Field South (CDFs), respectively, provide an unique resource of data to study the distant universe. The two fields cover a total area of about  $300 \text{ arcmin}^2$ , and have now been imaged with all the largest available telescopes (Hubble, Spitzer, VLT, Chandra, XMM, Herschel, CFHT). The GOODS HST Treasury Program (Gialavisco et al. 2004) provides ultra-deep high-resolution images in B-, V-, i- and z-bands. Deep ground-based imaging in the U-band is provided by VIMOS/VLT for the CDFS (Nonino et al. 2009), and at the Kitt Peak National Observatory for the HDFN. Moreover,

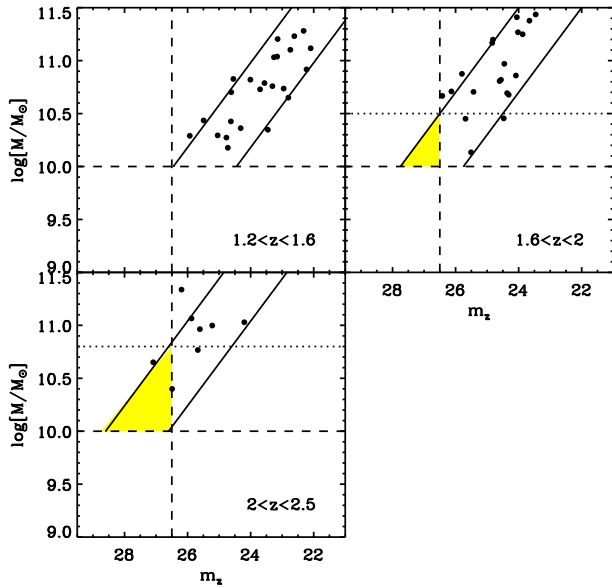


FIG. 2.— AB magnitude in the ACS/ $z$ -band band versus stellar mass, for galaxies in our sample at  $z > 1.2$ , divided in three smaller redshift bins ( $1.2 < z < 1.6$ ,  $1.6 < z < 2$  and  $2 < z < 2.5$ ). The vertical dashed line at  $m_z = 26.5$  indicates the magnitude at which the GOODS  $z$ -band images are 80% complete, the dashed horizontal line at  $M/M_\odot = 10^{10}$  shows our mass limit, and the dotted horizontal lines at  $M/M_\odot = 10^{10.5}$  and  $M/M_\odot = 10^{10.8}$  show the limit above which the  $1.6 < z < 2$  and  $2 < z < 2.5$  are complete, respectively. The diagonal lines indicate, for each redshift bin, the mass vs  $m_z$  relation for the reddest and bluest models available in our template grid. The yellow triangles at  $z > 1.6$  show the regions of the plane in which our selection is incomplete.

VLT/ISAAC imaged the CDFS in J-, H- and K-bands, while CFHT/WIRCAM imaged the HDFN in J- and K-bands (Lin et al. in prep; also see Wang et al. 2010). Ultradeep Spitzer/IRAC imaging is also available in the 3.6, 4.5, 5.6 and 8.0  $\mu\text{m}$  NIR channels.

We built a multiwavelength catalog (GUTFIT, Grand Unified TFIT catalog) for each of the GOODS-N and GOODS-S using the TFIT procedures by Laidler et al. (2007). This procedure allows to PSF match images having different resolutions, and uses the ACS/ $z$ -band (version 2.0) as detection image. The positions and profiles of galaxies in the ACS/ $z$ -band high resolution image are used as a prior to reconstruct the flux in the lower resolution images. This is useful for objects that are deblended in the high resolution images but are close enough in the sky to overlap in the low resolution ones. In this cases, TFIT is able to reconstruct the flux of each object, and is accurate down to the limiting sensitivities of images (Laidler et al. 2007).

We included all the WFC3 data available in the GOODS-South field to July 2010, namely the HUDF observations (GO 11563, PI: Illingworth) and the Early Release Science Program 2 (ERS2: GO 11359, PI: McConnell; see Windhorst et al. 2011 for further details). The former observed one WFC3 field ( $\sim 4 \text{ arcmin}^2$ ) centered in the HUDF in the F105W ( $Y$ ), F125W ( $J$ ) and F160W ( $H$ ) filters, imaged respectively for 16, 16 and 28 orbits, reaching  $1 - \sigma$  fluctuations of 27.2, 26.6 and 26.3

$AB/\text{arcsec}^2$  in the three bands, respectively. The latter covers  $40 \text{ arcmin}^2$  on the north part of the GOODS South field, imaged with the same filters as the HUDF/WFC3, with integration times of 2, 2 and 3 orbits respectively for the F105W ( $Y$ ), F125W ( $J$ ) and F160W ( $H$ ) filters, producing  $1 - \sigma$  fluctuations of 25, 24.4 and 24.1  $AB/\text{arcsec}^2$  in the three bands, respectively. We used a version of these datasets that had been processed as described in more detail in Koekemoer et al. (2011), which were combined using MultiDrizzle (Koekemoer et al. 2002) to a  $0.06''$  pixel scale, aligned to the existing GOODS and HUDF astrometric grid, and obtaining a PSF of  $\sim 0.16''$  in our resulting WFC3 images.

The sample was complemented with the 6000 spectroscopic redshifts available to date (3000 in the South and 3000 in the North), among which 2500 are at  $z > 1$  (Cimatti et al. 2008; Vanzella et al. 2008; Popesso et al. 2009).

We fitted the Spectral Energy Distribution of the galaxies in the two samples to measure accurate photo- $z$ , using the PEGASE 2.0 templates (Fioc & Rocca-Volmerange 1997). By comparing photo- $z$  and spectro- $z$ , we estimate that the scatter of our photo- $z$  is of the order of  $\sigma[\Delta z/(1+z)] \sim 0.04$ .

Once a redshift has been assigned to each galaxy (either spectroscopic or photometric), we fitted the SEDs from the UV to  $8\mu\text{m}$  to a set of models by Charlot & Bruzual 2009 (CB09, in preparation), in order to get accurate measurements of the stellar mass,  $E(B-V)$ , age and Star Formation Rate of sources. In particular, we use a Salpeter IMF (Salpeter 1955) with lower and upper mass of 0.1 and  $100 M_\odot$ , we apply the Calzetti law (Calzetti et al. 2000) to describe the dust extinction and we use exponentially declining Star Formation Histories. Maraston et al. (2010) showed that these models tend to overestimate the SFRs and underestimate stellar masses for a sample of star-forming galaxies at  $z \sim 2$ , and that exponentially increasing SFH give instead less biased results. We will explore if such biases are present for early-type galaxies as well in a forthcoming paper. The stellar mass that we derive does not include the mass loss from stars, but includes the stellar mass of remnants (white dwarfs, neutron stars, etc.). The Specific Star Formation Rates (SSFR), i. e. the star formation rate for unit mass, are derived by dividing the star formation rates by stellar masses. The stellar masses (and all the derived quantities) based on different IMFs that we cite and use as a comparison throughout the paper were homogenized to match our assumptions, using the offsets measured by Salimbeni et al. (2009):  $\log(M_{CB09}) = \log(M_{BC03}) - 0.2$  and  $\log(M_{Salp}) = \log(M_{Chab}) + 0.25$ , where BC03 stands for Bruzual & Charlot(2003). This process of homogenization is essential to ensure meaningful comparison among different samples at different redshifts.

We then extracted our sample of passive galaxies, selecting only objects with stellar mass  $M > 10^{10} M_\odot$  and  $\text{SSFR} < 10^{-2} \text{ Gyr}^{-1}$  at  $0 < z < 2.5$ . These criteria ensure that only the most massive and less star-forming objects at those redshifts are selected. This selection has resulted in a sample of about 900 candidate ETGs at redshifts between  $\sim 0.1$  and  $\sim 2.5$ . As we want to have an optical high-resolution image for each candidate, we

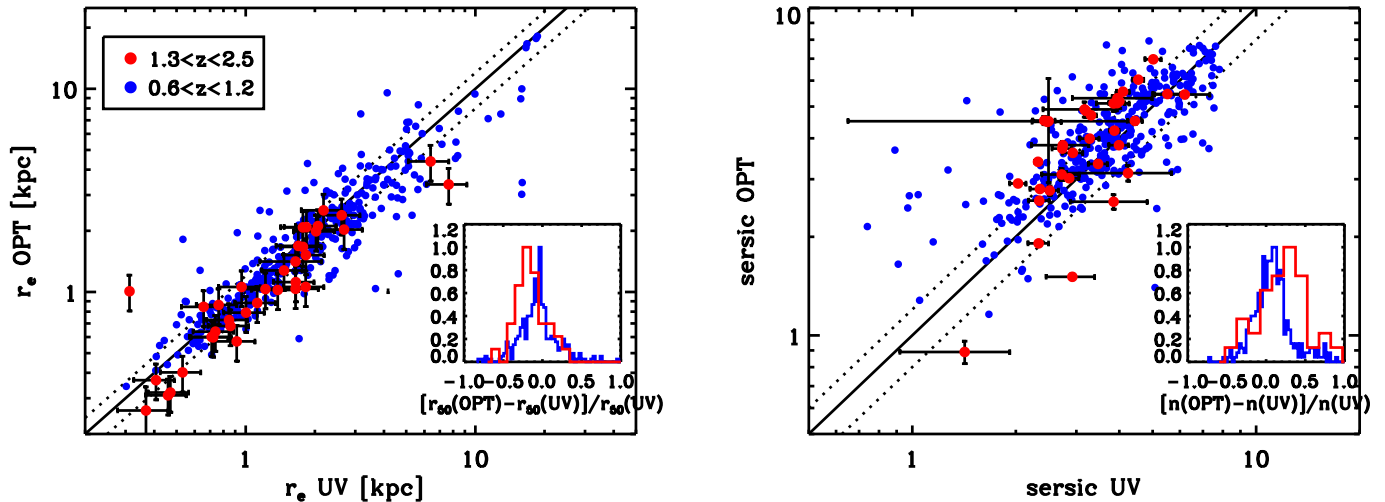


FIG. 3.— Comparison between the GALFIT best fit values in the optical and UV rest-frame for our sample of passive galaxies at  $z \sim 2$  (red) and the sample of passive galaxies at  $0.6 < z < 1.2$  (blue). The left and right panels show the half light radii and the Sérsic indices, respectively. The dotted lines show the  $\pm 20\%$  lines. The two insets show the distribution of the fractional differences between sizes and Sérsic indices in the optical and UV rest-frames.

kept only those  $z > 1.2$  galaxies that lie within either the ERS or HUDF WFC3 areas.

We visually classified both the  $z < 1.2$  and  $z > 1.2$  sample, in the  $z$ - and  $H$ -band respectively, and we kept only galaxies with a spheroidal morphology, i.e. galaxies with no signs of asymmetry and centrally concentrated. About 60% of all passive galaxies were classified as morphologically spheroidals, and were kept in the sample. We also checked the Spitzer/MIPS images, and we found a negligible fraction of objects detected at  $24\mu\text{m}$  ( $\sim 10$  objects at  $z < 1.2$  and 2 at  $z > 1.2$ ) that we removed from the sample. At the end, we end up with 563 passive galaxies, 52 of which are at  $z > 1.2$ . We stress once again that the 511 early-types at  $z < 1.2$  are extracted from the 300 arcmin<sup>2</sup> of GOODS-S&N, while the 52 at  $1.2 < z < 2.5$  are extracted from the ERS and HUDF WFC3 fields (for a total area of 49 arcmin<sup>2</sup>). Figure 1 shows the redshift distribution in the highest redshift bin,  $1.2 < z < 2.5$ , peaked around  $z \sim 1.6$ . 20 galaxies among the 52 in this redshift range have spectroscopic redshifts.

In Figure 2 we show the stellar mass as a function of the ACS/ $z$ -band magnitude for galaxies at  $z > 1.2$ , with the aim of assessing the incompleteness of our selection at those redshifts. For three redshift bins ( $1.2 < z < 1.6$ ,  $1.6 < z < 2$  and  $2 < z < 2.5$ ) we compare the stellar mass vs  $m_z$  of objects in the sample with the models used to fit their SEDs. By definition, we can detect in our sample only galaxies falling between the two diagonal lines in Fig 2, that represent the bluest and reddest models. We used a Montecarlo approach, simulating galaxies with deVaucouleurs profiles and different sizes, to establish the detection limit of the  $z$ -band imaging version 2.0 that is used by GUTFIT as detection image. The objects are then placed on the real  $z$ -band images, and the same SExtractor procedure used to extract real objects is run on the simulated images. Ignoring for now the dependence of the completeness on the size of the galaxies (that will be discussed in section 4), we find that our selection achieves 80% completeness at  $m_z = 26.5$ , for

compact objects. At  $1.2 < z < 1.6$  the mass vs  $m_z$  relation for the reddest model and the 80% completeness magnitude intersect around  $M/M_\odot = 10^{10}$ : this implies that up to  $z \sim 1.6$  we detect all passive galaxies with any color down to  $M/M_\odot = 10^{10}$ . At higher redshift the model and the 80% completeness line intersect at higher masses, implying that our selection misses part of the galaxies with  $M/M_\odot > 10^{10}$ . In particular, at  $1.6 < z < 2$  and at  $2 < z < 2.5$  our sample is complete only down to  $M/M_\odot > 10^{10.5}$  and  $M/M_\odot > 10^{10.8}$ , respectively.

For both the samples we used the GALFIT package (Peng et al. 2002) to fit the light profile in the rest-frame UV and optical to the Sérsic model

$$I(r) = I_e \exp \left\{ -b_n \left[ \left( \frac{r}{r_e} \right)^{1/s} - 1 \right] \right\}, \quad (1)$$

where  $I(r)$  is the surface brightness measured at distance  $r$ ,  $I_e$  is the surface brightness at the effective radius  $r_e$  and  $b_n$  is a parameter related to the Sérsic index  $s$ . For  $s=1$  and  $s=4$  the Sérsic profile reduces respectively to an exponential and deVaucouleurs profile. Bulge dominated objects typically have high  $s$  values (e.g.  $s > 2$ ) and disk dominated objects have  $s$  around unity. Ravindranath et al. (2006), Cimatti et al. (2008) and Trujillo et al. (2007) showed that GALFIT yields unbiased estimates of the Sérsic index and effective radius for galaxies with  $S/N > 10$  and  $r_e > 0.03''$ , independently of the redshift of the source, thus demonstrating that the surface brightness dimming is not an issue for this kind of studies.

The PSF was obtained in each passband needed by averaging well-exposed, unsaturated stars. We run GALFIT experimenting on various sizes of the fitting region around each galaxy, and with the sky either set to a pre-measured value or left as a free parameter. We verified that the sizes and Sérsic indices do not vary by more than 10% in the various cases. The values that we show

throughout the paper were obtained with a free sky and  $6 \times 6$  arcsec<sup>2</sup> fitting regions. Any closeby object detected by SExtractor within each fitting region was automatically masked out during the fitting procedure.

Finally, we selected a sample of local galaxies from the Sloan Digital Sky Survey (SDSS), for which masses, star formation rates and morphological parameters are available in literature. In particular, we combined the MPA SDSS DR7 catalog, that contains stellar masses and star formation rates (Kauffmann et al. 2003; Brinchmann et al. 2004) with the DR7 NYU Value-Added Galaxy Catalog, that contains the GALFIT Sérsic best fit to the  $u$ ,  $g$ ,  $r$ ,  $i$  and  $z$  SDSS images (Blanton et al. 2005). We defined the local sample of massive and passive early-type galaxies by applying the same criteria used for the high- $z$  ones: stellar mass  $M_{\odot} > 10^{10}$  and specific star formation rate  $\text{SSFR} < 10^{-2} \text{Gyr}^{-1}$ . Instead of visually inspecting the whole sample, we eliminated the disk dominated objects removing all the objects (5% of the total) with Sérsic index  $s < 2$  in the  $r$ -band. We verified with a random sample of 200 SDSS galaxies that the contamination of disk dominated objects among objects with  $s > 2$  is below 5%.

### 3. MORPHOLOGICAL PROPERTIES AS A FUNCTION OF THE REST-FRAME BAND

In Figure 3 we compare the Sérsic indices and the physical sizes in the UV and optical rest-frames, for the high and low redshift samples. Since the errors on the sizes and Sérsic indices given by GALFIT are the formal errors derived by the fitting procedure and do not take into account any systematic uncertainty, in this Figure and in the following we set the error bars to a minimum value of 20%. For the low redshift sample we restricted the analysis at  $z > 0.6$ , and we used the ACS  $v$ -band and  $z$ -band, matching the rest-frame UV and optical, respectively. We did not include galaxies at lower redshift, as the UV rest-frame at  $z < 0.6$  would be matched by the ACS/B-band, that provides a worse S/N than the other ACS bands. As we already said in the previous section, the  $z \sim 2$  sample contains the 52 galaxies for which the WFC3 imaging is available: at that redshift, the  $z$ - and the  $H$ -band correspond respectively to the rest-frame UV at  $\sim 3000\text{\AA}$  and optical at  $\sim 5700\text{\AA}$ . First of all, 95% of the passive galaxies at  $z < 1.2$  and  $z \sim 2$  have a Sérsic index  $s > 2$ , both at UV and optical wavelengths. This is not surprising, as the sample has been restricted to contain only visually classified spheroidals. Secondly, the sizes measured in the UV and in the optical correlate almost perfectly with each other, with a scatter smaller than  $\pm 20\%$ . The Sérsic indices in the two rest-frame bands are correlate as well, but show a larger scatter ( $\sim 40\%$ ). However, we do see systematic offsets for both sizes and Sérsic indices in the two rest-frames, that become more evident when checking the fractional differences between optical and UV, shown in the insets of Figure 3. We see that on average galaxies at  $1.2 < z < 2.5$  have sizes 20% smaller and Sérsic indices 25% larger in the optical than in the UV rest-frame. Similarly, galaxies at  $0.6 < z < 1.2$  galaxies have sizes 10% smaller and Sérsic indices 10% larger in the optical than in the UV rest-frame.

This reinforces our previous result presented in Cassata et al. (2010), where we showed a similar trend for the subset of galaxies at  $z \sim 2$  lying in the HUDF,

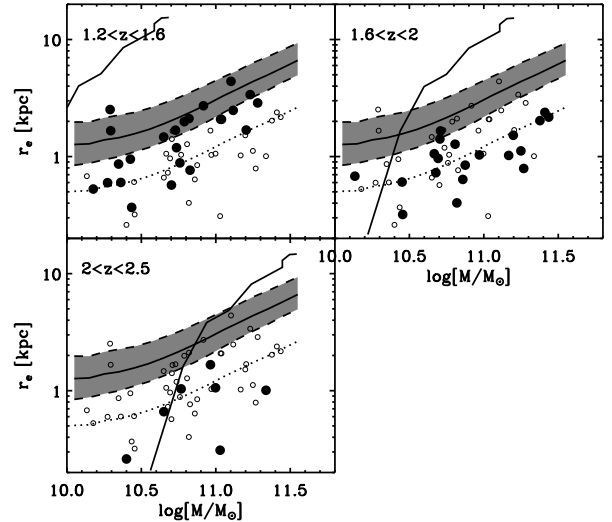


FIG. 4.— The mass size relation in the optical rest-frame for the galaxies at  $z > 1.2$  extracted from the HUDF+HUDF WFC3 fields, in three redshift bins:  $1.2 < z < 1.6$ ,  $1.6 < z < 2$  and  $2 < z < 2.5$ . The black filled circles indicate objects in that redshift bin, while empty circles represent galaxies in the other two redshift bins, for comparison. In all panels, the gray filled region indicates the locus occupied by SDSS passive galaxies at  $0 < z < 0.1$ : the continuous line shows the median of the distribution, while the dashed black lines contain 68% of the objects. The black dotted line corresponds to the locus of galaxies 0.4 dex smaller than local counterparts: galaxies below the line are considered ultra-compact according to our definition. The black continuous curves encompass the region of the plane where our selection detects at least 80% of the galaxies. Galaxies left of the line have surface brightnesses too low to be detected.

and it is in good agreement with other studies of early-type galaxies at  $z \sim 2$  (McCarthy et al. 2007; Trujillo et al. 2007; Ryan et al. 2011), as well as at lower redshift (Papovich et al. 2003; Cassata et al. 2005).

Interestingly, these biases basically imply that early-type galaxies at  $z > 1.2$  show a negative color gradient, with the center being redder than the outskirts. Early-types at lower redshift show a similar, but shallower, color gradient. This is in very good agreement with the results by Guo et al. (2011b), who found negative color gradients for 6 passive galaxies in HUDF, steeper than those observed in local early-type galaxies.

Based on these evidences, we can conclude that in the whole  $0 < z < 2.5$  interval the morphological K-correction is weak for passive spheroidals that have already ended their star formation activity.

### 4. THE MASS-SIZE RELATION FOR EARLY-TYPE GALAXIES AT $0 < z < 2.5$

In Figure 4 we show the mass-size relation for the 52 galaxies at  $1.2 < z < 2.5$  selected in the ERS+HUDF WFC3 fields, in the same three redshift bins of Figure 2. The sizes have been measured by GALFIT in the F160w filter, that at these redshifts corresponds to the optical rest-frame regime. We plot as well the mass-size relation for local ETGs drawn from the SDSS, in the same optical rest-frame. We stress that here the mass



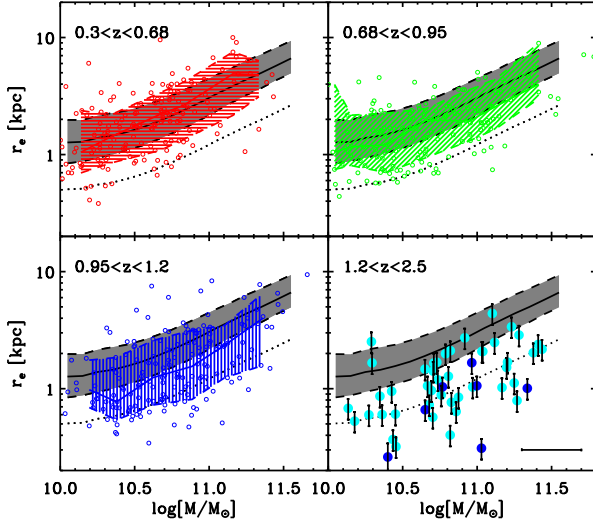


FIG. 5.— The mass size relation in the optical rest-frame for in four redshift bins:  $0.3 < z < 0.68$ ,  $0.68 < z < 0.95$ ,  $0.95 < z < 1.2$  and  $1.2 < z < 2.5$ . For the first three bins we used the  $z$ -ACS band, while for the last we used the  $F160W$ -WFC3 band. The first three bins are designed to contain roughly the same number of galaxies. In all bins, the gray filled region indicates the locus occupied by SDSS passive galaxies at  $0 < z < 0.1$ : the continuous line shows the median of the distribution, while the dashed black lines contain 68% of the objects. The black dotted line corresponds to the locus of galaxies 0.4 dex smaller than local counterparts: galaxies below the line are considered ultra-compact according to our definition. In the first three panels the colored regions indicate the distribution of the passive galaxies in each redshift bin: the continuous colored line indicates the median of the distribution, and the dashed lines contain 68% of the galaxies. The empty color circles indicate individual galaxies. For the highest redshift bin, we show each galaxy with its error bar on the physical size: cyan and blue points indicate galaxies at  $1.3 < z < 2$  and  $2 < z < 2.5$ , respectively. The error bar at  $\log[M/M_\odot] = 11.5$  and  $r_e = 0.2 kpc$  shows the typical error on the mass estimates.

measurements were homogenized to a Salpeter IMF (see Section 2 for details). The relation for SDSS passive galaxies is found to be in good agreement with results by Shen et al. (2003), that are widely used by many authors as a reference at  $z \sim 0$ . At all redshifts, we call *ultra-compact* any early-type galaxies 0.4 dex smaller than local SDSS galaxies of the same mass, and *compact* any galaxy 1- $\sigma$  below the local relation. The first definition comes out naturally as the maximum size without a counterpart in the local universe (see Section 5); the second is the least strict definition of *compactness* used in the literature and in this way we can compare our measurements with others. The *normal* ETGs are those lying on top or above the local relation. If we define the mean mass density within the half light radius as:

$$\Sigma_{50} = \frac{0.5M_*}{\pi r_e^2} \quad (2)$$

we note that the local relation is roughly parallel to the loci of constant  $\Sigma_{50}$ . Compact and ultra-compact ETGs have mass densities  $\Sigma_{50} \gtrsim 3 \times 10^9 M_\odot kpc^{-2}$  and  $\Sigma_{50} \gtrsim 1.2 \times 10^{10} M_\odot kpc^{-2}$ , respectively.

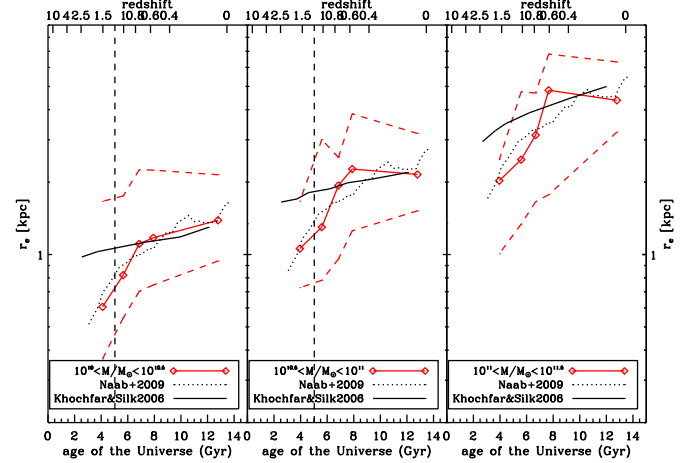


FIG. 6.— Evolution of the average size for passive galaxies at  $0 < z < 2.5$ , for 3 mass intervals:  $10^{10} < M/M_\odot < 10^{10.5}$  (left),  $10^{10.5} < M/M_\odot < 10^{11}$  (center) and  $M/M_\odot > 10^{11}$  (right). The dashed lines represent the 1- $\sigma$  scatter, i.e. they contain 68% of the objects. The dotted line is the size evolution for a galaxy with a final mass at  $z \sim 0$  of  $M/M_\odot \sim 10^{11}$  that grows via minor merger modeled via a high-resolution hydrodynamical simulation by Naab et al. (2009), and the continuous line shows a semi-analytical model by Khochfar & Silk (2006). The datapoints left of the vertical line at  $z = 1.2$  are not complete in the first two mass regions.

For each redshift bin we show the region of the plane where our selection detects at least 80% of the objects. To build this region we took the reddest template available in our sample, for which we know, at every redshift, the  $z$ -band magnitude as a function of the stellar mass (see Fig. 2). We combine this with the output of the Montecarlo simulation that we used to assess the completeness of the  $z$ -band detection images: in particular, we know the fraction of retrieved objects as a function of the magnitude  $m_z$  as well as of the half-light radius  $r_e$ . Finally, we built, at each redshift bin, the locus of the 80% completeness limit in the stellar mass vs  $r_e$  plane. The detection fraction at smaller masses or larger sizes of this model drops really quickly: in practice, objects left of this line can not be detected by our selection method (the few objects lying out of the forbidden region are bluer than the extreme template we used for this exercise); on the other hand, this work ensures that we detect at least 80% of the objects lying to the right of the line. At  $1.2 < z < 1.6$ , our sample is complete down to  $M = 10^{10} M_\odot$  (as already discussed in section 2, fig. 2 and up to  $r_e \sim 3 - 10$  (depending on the mass). At  $1.6 < z < 2$  the limit moves to higher masses, but still we can detect 80% of the galaxies with  $M > 10^{10.4} M_\odot$  and sizes  $r_e \sim 3 - 10$ . Finally, at  $2 < z < 2.5$  we can detect 80% of the galaxies with  $M > 10^{10.8} M_\odot$  and sizes  $r_e \sim 3 - 10$ .

The first interesting result is that at  $1.2 < z < 1.6$ ,  $1.6 < z < 2$  and  $2 < z < 2.5$  respectively about 65%, 95% and 100% of early-type galaxies are more than 1- $\sigma$  below the local relation, and that about 25%, 50% and 80% are ultracompact, according to our definition. The evolution of these fractions between  $1.2 < z < 2.5$  seems to be real: in fact, even considering only the part of the plane where the detection is higher than 80%, the re-

sult still holds. In particular, at  $M \gtrsim 10^{10.6-8} M_\odot$ , we should detect “normal” ETG with  $r_e \sim 2 - 4$  kpc at  $z > 1.6$ , if they were present, but we detect none. However, since at  $z > 1.6$  we might progressively miss more and more large galaxies, it is possible that the compact and ultra-compact fractions at those redshifts are slightly over-estimated. In the following sections and figures, in order to improve the statistics, we will combine the three redshift bins of Figure 4 in one. Note that the absence in our sample of very massive galaxies with large size is due to their rarity, as with a surface density of one every  $\sim 500$  arcmin<sup>2</sup> (Mancini et al. 2010) one does not expect to find any in the 40 arcmin<sup>2</sup> covered by the WFC3 data.

At  $1.2 < z < 2.5$ , passive galaxies appear to be on average 3–5 times smaller than local counterparts of the same mass. This result is in good agreement with our previous findings in Cassata et al. (2010) and with Ryan et al. (2011), obtained with WFC3 in the ERS and/or HUDF surveys. This result is also in agreement with previous studies at high- $z$  using NICMOS data (Toft et al. 2007; Zirm et al. 2007; Van Dokkum et al. 2008; Buitrago et al. 2008) and ACS data (Trujillo et al. 2007; Cimatti et al. 2008). However, we do not find evidence for a population of “normal” passive  $z \sim 2$  galaxies as abundant as the one presented by Saracco et al. (2009; 2010): they claim that  $\sim 60\%$  of all early-types at  $1 < z < 2$  are indeed on top of the local relation. This discrepancy may in part be due to the slightly different redshift interval they use: if we select passive galaxies in the same redshift interval used by Saracco et al. (2010),  $0.9 < z < 1.92$ , we find a fraction of compact galaxies of  $\sim 60\%$ . Moreover, we note that Saracco et al. (2009) claim that the *normal* early-types at  $z \sim 2$  (i.e. those lying on the local relation) have much younger ages than the *compact* ones. It is possible that we do not select such young early-type galaxies because of our very conservative SSFR selection ( $SSFR < 10^{-2} \text{Gyr}^{-1}$ ). We also note that Mancini et al. (2010) find a predominance of *normal*-size ETGs in a sample of 12 very massive such galaxies at  $1.4 < z_{\text{phot}} < 1.7$ , with  $M > 2.5 \times 10^{11} M_\odot$  (Chabrier IMF), a mass range which is not reached by the present sample.

We thus confirm that passive galaxies at  $z \sim 2$  are on average smaller than local counterparts, at least in the mass range  $10^{10} < M/M_\odot < 10^{11}$  in which our sample is representative, but we also confirm that compact and normal-size galaxies coexist up to this high redshift. The aim of this work, however, is to follow the global evolution of the passive galaxies in the mass-size plane from  $z \sim 2.5$  to  $z \sim 0$ , using for the first time an homogeneous and complete dataset. The evolution at  $z < 1.2$  is illustrated by Fig. 5, where we show the mass-relation for 4 redshift bins:  $0.3 < z < 0.68$ ,  $0.68 < z < 0.95$  and  $0.95 < z < 1.2$  and  $1.2 < z < 2.5$  (the fourth combines together the 3 redshift bins of Figure 4). It is evident that the average mass-size relation evolves continuously from  $z \sim 2$  to  $z \sim 0$ . This migration is almost completed by  $z \sim 0.4$ , as shown in the first panel of Fig. 5, where the distribution of galaxies is somehow overlapping with the  $z \sim 0$  SDSS relation (although the scatter is larger for the  $0.3 < z < 0.68$  galaxies). The fraction of “compact” galaxies, defined as the galaxies that at each redshift lie

$1 - \sigma$  below the local relation (the gray strip in Fig. 5) drops from  $z \sim 2$  to  $z \sim 0$  following such evolution, as we will see in more detail in the next Section.

Figure 6 shows the evolution of the average size of passive galaxies between  $z \sim 2$  and  $z \sim 0$  for three different mass intervals:  $10^{10} < M/M_\odot < 10^{10.5}$ ,  $10^{10.5} < M/M_\odot < 10^{11}$  and  $M/M_\odot > 10^{11}$ . We stress that at  $1.2 < z < 2.5$  the sample is only complete down to  $M/M_\odot = 10^{10.8}$ .

It is clear, once again, that the evolution is faster at  $z > 0.6$  (or age of the universe  $< 6 - 8$  Gyr), while at  $z < 0.6$  the average sizes remain almost unchanged. Our results are in quantitative agreements with Stott et al. (2011), who claimed that the average size of the most massive ETGs increases by 30% from  $z \sim 1$  to  $z \sim 0$ . The shape of the evolution, in a logarithmic plane, is similar for the three mass bins, so the *fractional* size increment as a function of the cosmic time appears to be independent of the stellar mass. This implies that on a linear scale the size evolution is faster for the most massive galaxies than for less massive ones, in agreement with Ryan et al. (2011).

We note also that the evolution of the average size from  $z \sim 2$  to  $z \sim 0$  is in qualitative agreement with the prediction by Naab et al. (2009), who modeled the formation and evolution of a passive galaxy with a final mass of  $1.5 \times 10^{11} M_\odot$  in a high-resolution hydrodynamical simulation. In such simulation, the mass of the galaxy increases by a factor of 2 from  $z \sim 2$  to  $z \sim 0$  through a series of minor merger events, that at the same time are responsible for the decrease of the stellar density and increase of the size throughout the same redshift interval. The observed size evolution is not well reproduced by the model by Khochfar&Silk (2006), who used a semianalytical technique in which the size evolution is the result of the amount of cold gas available during major merger events.

## 5. EVOLUTION OF THE NUMBER AND MASS DENSITY OF PASSIVE GALAXIES

In the previous section we have observed that the average mass-size relation of passively evolving early-type galaxies undergoes significant evolution from  $z \sim 2$  to the present.

In principle, one can imagine that the evolution is driven by two independent mechanisms: one is the progressive appearance, as time evolves, of new early-type galaxies due to the cessation of the star-formation activity; the other is the evolution of galaxies that are already passive, and whose stellar populations remains mostly passive, but whose mass and size change as the result of merging and interactions with other galaxies, passive or otherwise. Some models including these effects have been proposed recently: Khochfar&Silk (2006) suggested that the observed size evolution of passive galaxies can be explained by the variation of the amount of cold gas available during the major merger events that originate early-type galaxies: the most massive ones formed at high- $z$ , when major mergers were more gas rich than at later epochs. Naab et al. (2009), on the other hand, introduced a model in which the size of a passive galaxy increases, as time goes by, through the continuous merging activity with low mass objects.

At any redshift, the appearance of new passive galax-

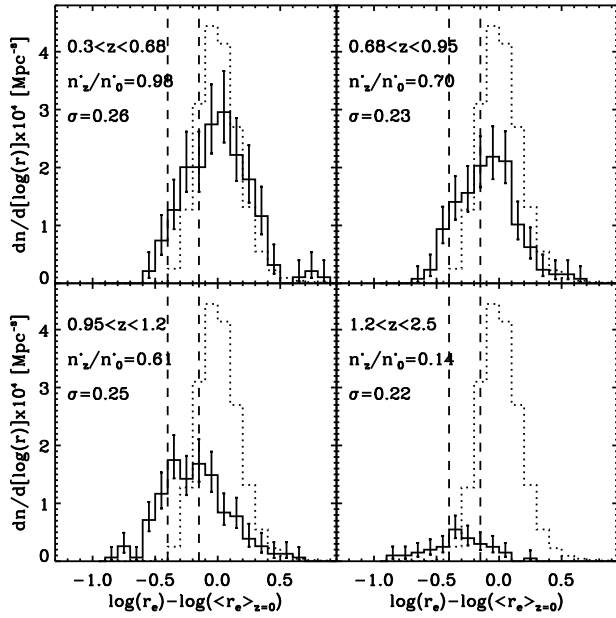


FIG. 7.— For each of the four redshift bins of Figure 6 we report the histograms of the ETGs sizes. In particular, for each galaxy we calculated the ratio between its size and the average size of local ETGs of the same mass. The histograms are normalized to the number density of ETGs in each redshift bin (solid line). The dotted line is the size histogram for early-type galaxies in SDSS. The error bars reflect the Poisson noise in each size bin. The vertical dashed lines at  $\log(r_e) - \log(\langle r_e \rangle_{z=0}) = -0.15$  and  $\log(r_e) - \log(\langle r_e \rangle_{z=0}) = -0.4$  indicate our definition of *compact* and *ultra-compact* ETGs given in Section 2. In each panel,  $n_z^*$  and  $n_0^*$  indicate the number density of ETGs in that redshift bin and in the local Universe, respectively. For each panel,  $\sigma$  indicates the standard deviation of the size distribution, to be compared with  $\sigma = 0.17$  for the SDSS  $z = 0$  galaxies.

ies modifies the mass-size relationship depending on the mass and size distribution of the galaxies that become passive. On the other hand, the morphological transformation of the old passive galaxies contributes to modify the mass-size relationship depending on how galaxies accrete stellar mass and/or grow in size, for example either increasing stellar mass but remaining unchanged in size, or also growing by “puffing-up” (e.g. Hopkins et al. 2009).

Van der Wel et al. (2009) found that in the local universe small passive galaxies with  $M > 10^{11} M_\odot$  are older than the larger ones, implying that at higher redshift such larger galaxies gradually disappear. They suggest that this effect, together with some dry merging activity, may account for the observed size evolution from  $z \sim 2$  to  $z \sim 0$ .

In this paper, we document the evolution of the mass-size relation in terms of the relative importance of the size growth of individual passive galaxies and the appearance of new large ETGs at more recent epochs. To this purpose, we constrain the number density of ETGs for different sizes as a function of the redshift. We stress that up to date the evidence that compact early-type galaxies are more common at high- $z$  than in the local Universe is mainly based only on the fact that their “fraction” increases with  $z$ , irrespectively of the fact that the total

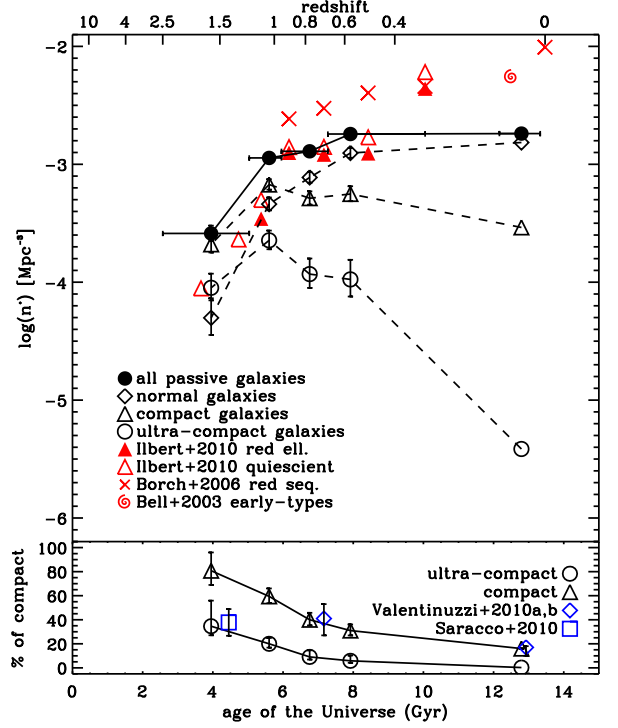


FIG. 8.— *Top panel*: number density as a function of the age of the universe and redshift of passive galaxies with  $M > 10^{10} M_\odot$ . Filled circles indicate the mass density for all massive passive galaxies in our sample; the empty triangles represent the mass density in compact passive galaxies, defined as the objects lying  $1 - \sigma$  below the local SDSS relation (or equivalently with  $\Sigma_{50} > 3 \times 10^9 M_\odot$ ); empty circles represent ultra-compact galaxies, those galaxies 0.4 dex smaller than local counterparts; empty diamonds indicate the number density in normal passive galaxies, i.e. galaxies that reside on the local mass-size relation. The points at  $z \sim 0.1$  have been derived using the local SDSS sample defined in Section 2. Red symbols are literature results at different redshifts, obtained integrating the best fit Schechter functions down to  $M = 10^{10} M_\odot$ : filled and open triangles are results by Ilbert et al. (2010) for red ellipticals and quiescent galaxies ( $\text{SSFR} < 10^{-2} \text{ Gyr}^{-1}$ ), respectively; red crosses are measurements by Borch et al. (2006) for galaxies in the red sequence; the red spiral indicates the local value estimated by Bell et al. (2003) in the local Universe for early-type galaxies, defined as the objects with concentration  $c_r > 2.6$ . *Bottom panel*: Fraction of passive galaxies that are also compact (triangles) and ultracompact (circles), as a function of the age of the universe or the redshift.

number of ETGs is not constant throughout the life of the Universe (e.g. Trujillo et al. 2009). Nevertheless, some authors (Valentinuzzi et al. 2010a,b; Taylor et al. 2010; Saracco et al. 2010) have compared the *number density* of compact ETGs at  $z \sim 2$  and  $z \sim 0$ , but they used non homogeneous samples of ETGs selected with different techniques at high- and low- $z$ . In this work, for the first time, we select in an homogeneous way a mass complete sample of ETGs and we measure the number density of compact and normal ETG throughout the entire  $0 < z < 2$  redshift range.

We used a simple  $V/V_{max}$  formalism to measure the number and mass densities in early-types with  $M > 10^{10} M_\odot$  in the same four redshift of Figure 5 and for the local SDSS sample at  $z \sim 0$ . Our sample is complete down to this mass limit just to  $z = 1.6$ , while at  $z > 1.6$  the sample is only complete down to  $M = 10^{10.8} M_\odot$  (see Fig. 2). The  $V/V_{max}$ , however, takes into account



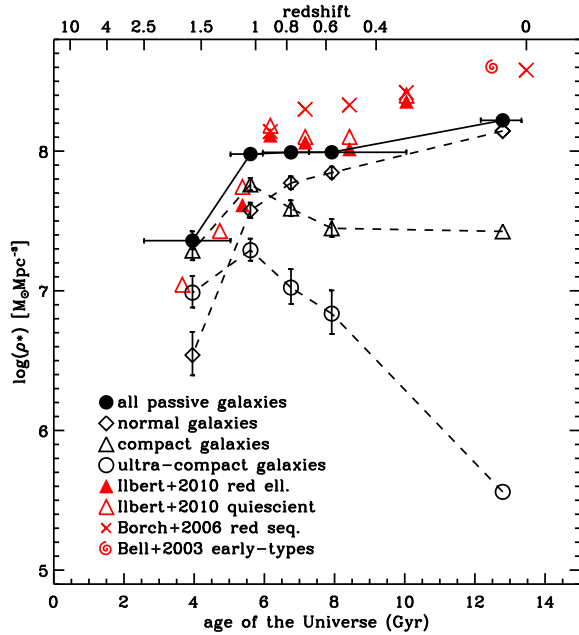


FIG. 9.— Stellar mass density as a function of the age of the universe and redshift of passive galaxies with  $M > 10^{10} M_{\odot}$ . The symbols are the same as in Figure 8

such incompleteness and corrects for it. In particular, our method assumes that the density of galaxies in the yellow region of Fig. 2 is the same as the one that we measure for galaxies with  $m_z < 26.5$ .

In Figure 7 we show the size distribution of ETGs in the same four redshift bins as Figure 5, scaled to the number density of galaxies in each bin and compared with the distribution of galaxies in the local universe derived from our SDSS sample. For each galaxy in the GOODS and SDSS sample we calculated the ratio of its size to the average size of SDSS ETGs with the same stellar mass, and then we plotted the histograms of such ratio. The local size distribution is almost perfectly lognormal, with virtually no *ultra-compact* ETGs (e.g. galaxies with sizes 0.4 dex smaller than the local average). However, some authors suggested that a compact population of ETGs could be hidden among unresolved red objects in SDSS, and thus their number density could be somewhat underestimated (Valentinuzzi et al. 2010a; Shih & Stockton 2011). The size distribution at higher redshift is approaching a lognormal as well, even though it is broader than the  $z \sim 0$  one. The standard deviation of the distribution is in fact  $\sigma \sim 0.22 - 0.26$  at  $0.3 < z < 2.5$ , while it is  $\sigma \sim 0.17$  at  $z \sim 0$ . This effect might be due to the fact that  $z > 0.3$  size measurements are noisier than the  $z \sim 0$  ones, thus producing a broader distribution.

The bottom right panel of Fig. 7 shows that at the same stellar mass ETGs at  $1.2 < z < 2.5$  are on average 0.5 dex smaller than their local counterparts. This indicates that early-type galaxies assembled at those epochs are preferentially small. Note that we are not suggesting that the size distribution at high redshift is truncated: galaxies with large size become rarer at  $z > 1.2$ , implying that surveys with larger area coverage than ours are required to find them in significant numbers (e.g. Mancini et al. 2010).

By redshift  $z \sim 1$ , the number density of ETG has increased by a factor of 5 (see also Figure 8). We note that the number density of ETGs increased significantly at all sizes from  $1.2 < z < 2.5$  to  $0.95 < z < 1.2$ : if for a moment assume that the galaxies already present at  $z > 1.3$  do not grow in size, the ETGs formed during this epoch would have a size distribution spanning from -0.5 dex smaller to 0.5 dex larger than local counterparts. This indicates that the new galaxies formed over this period have typically larger sizes than those already present at  $z > 1.2$ . Even though the size distribution in the  $0.95 < z < 1.2$  bin is significantly different than the local one, the number density of galaxies 0.3 dex larger than local counterparts is now similar to the local value.

The evolution at later epochs is much milder, with the histogram progressively skewing towards larger sizes, and with the total number density of ETGs increasing by a factor of  $\sim 1.5$ . The ultra-compact objects, i.e. those with size 0.4 dex smaller than local counterparts, gradually disappear, while the number of galaxies with sizes comparable to the local value ( $\log(r_e) - \log(\langle r_e \rangle_{z=0}) \sim 0$ ) steadily increases. This indicates that in this phase the smallest galaxies grow in size, and that the new galaxies formed have sizes comparable to the local counterparts. We note that the evolution in the lowest redshift bin is not yet complete: even though the peak of the histogram is close to the peak of the local SDSS one, and the tail at large size is quite similar to the local one, still some ultra-compact galaxies are present. In the next 5 Gyr, i.e. between  $z \sim 0.5$  and  $z \sim 0$ , they keep growing in size and reach the present distribution, with essentially negligible new ETGs added (the area enclosed by the two histogram is almost the same, see also Figure 8). As already noted before, the size distribution at  $z \sim 0$  is much narrower than that at  $0.3 < z < 2.5$ : this can be in part due to the errors on the size measurements at high- $z$ . However, while the distribution at large sizes is quite similar at  $z > 0.3$  and  $z \sim 0$  (and the small difference can be explained with a 5% of outliers), the excess of small galaxies at  $z > 0.3$  is much more significant, and, if not true, would imply a unlikely large number of small size outliers (50% of the objects at  $z > 1.2$  and 15–20% at  $0.3 < z < 1.2$ ).

Figures 8 and 9 show the evolution of the number density  $n^*$  and stellar mass density  $\rho^*$  contributed by normal, compact and ultra-compact ETGs with  $M > 10^{10} M_{\odot}$  as a function of redshift and cosmic time, together with the evolution of the fraction of passive galaxies that are also compact and ultra-compact (bottom panel in Figure 8). The data at  $\langle z \rangle = 0.1$  have been derived using the SDSS local sample defined in Section 2. Our high- and low- $z$  samples probe  $\sim 6$  Gyr of cosmic time, from the epoch when the Universe was 4 Gyr old to the epoch it was 10 Gyr old. Including the point at  $z \sim 0$ , we can follow the evolution up to 13.6 Gyr after the Big Bang.

In order to estimate a reliable error to assign to the mass and number density at each redshift we used a simple Monte Carlo simulation. In particular, we built 1000 realizations of our sample by perturbing the stellar mass of each galaxy assuming a typical (quite conservative) random error of  $\pm 0.4$  dex, and we thus measured 1000 realizations of the mass density as a function of the redshift. In Figs. 8 and 9 we use the median and standard

deviation of such 1000 measurements as the value of the mass density and relative error, that thus do not include any estimate of the cosmic variance.

We compared our measurements with results in the literature for samples of similarly selected passive galaxies. In particular, we took the best fit Schechter parameters by Ilbert et al. (2010), Borch et al. (2006) and Bell et al. (2003), we homogenized their masses to our assumptions and we integrated their Schechter function down to our mass limit ( $M_* > 10^{10} M_\odot$ ), in order to have homogeneous measurements. However, since the mass functions of passively evolving galaxies have all moderate slopes at low mass values, both the number density  $n^*$  and the mass density  $\rho^*$  are dominated by galaxies around  $M^*$ , that is typically  $M^* \simeq 10^{10.6} M_\odot$  (Ilbert et al. 2010; Peng et al. 2010). Thus, the contribution to the number and mass density of galaxies with  $M^* < 10^{10} M_\odot$  is negligible, and the values presented here can be considered total values. The measurements by Saracco et al. (2010) are instead for galaxies with  $\sim 4.5 \times 10^9 M_\odot$ , but again this different limit should not affect our comparison. The incompleteness of our sample at  $z > 1.2$  do not strongly affect the conclusions of this discussion. Even if we eliminated all galaxies with  $z > 1.6$  (the redshift at which the sample is complete down to  $M = 10^{10} M_\odot$ ), we would have found a comparable number density of ETGs.

Our results for the global population of passive galaxies at  $0.5 < z < 2.5$ , both in Figure 8 and 9 are in fair agreement with the results for quiescent and red elliptical galaxies by Ilbert et al. (2010). We do see, however, a gap between our measurements at  $z < 1$  and those by Borch et al. (2006) and Bell et al. (2003). These differences are probably due to the different selection criteria: our selection is very conservative, and just at all redshifts selects galaxies with a tight upper limit to their SFR, and an early-type morphology, whereas Borch et al. (2006) refer to the mass density for all galaxies on the red sequence, that can be easily contaminated by dusty star forming galaxies (Cassata et al. 2008). On the other hand, Bell et al. (2003) select as early-types the galaxies with concentration in the  $r$ -band  $c_r > 2.6$ , that can thus be contaminated by bulge-dominated spirals.

By comparing Figure 8 and Figure 9 we can draw interesting conclusions on the evolution of the passive population from  $\langle z \rangle = 1.6$  to  $z \sim 0$ . In particular, both the mass density and the number density of early-type galaxies increases by a factor of  $\sim 5$  from  $\langle z \rangle = 1.6$  to  $z \sim 1$ , similarly to what has been found by Franceschini et al. (2006), Arnouts et al. (2007) and Abraham et al. (2007). This indicates that the bulk of the quenching of star formation if such galaxies takes place around that epoch. The evolution at later epochs is much milder. While the number density increases by a factor of 1.5 between  $z \sim 1$  and  $z \sim 0.5$ , the mass density remain constant over the same interval. This implies that new early-type galaxies are constantly added from  $z \sim 1$  to  $z \sim 0.5$ , as already seen in Figure 7, but they are not massive enough to modify significantly the mass density. In other words, the new early-type galaxies added from  $z \sim 1$  to  $z \sim 0.5$  are low mass objects, in good agreement with the “downsizing” scenario for the evolution of such galaxies (e.g., Thomas et al. 2010). We note that the

data by Ilbert et al. (2010) show a similar behavior.

However, we can not draw any strong conclusions, based on our data, on the evolution of the number density and mass density of ETGs from  $z \sim 0.5$  (the smallest GOODS redshift bin) and  $z \sim 0$  (the local SDSS value), since the GOODS fields are too small to minimize the effects of the cosmic variance.

Figures 8 and 9 distinguish the number and density evolution of compact, ultra-compact and normal ETGs as a function of redshift. In particular, Figure 8 shows that the number densities of the *compact* and *ultra-compact* ETGs are not constant through the explored redshift range. We stress that at  $z \sim 0$  the classical definition of compactness sets to 16% the fraction of *compact* galaxies. At first, the number densities of compact and ultra-compact ETGs increase following the strong evolution the global passive population: by  $z \sim 1$  there appears to be  $\sim 3$  times more compact and ultra-compact galaxies than those we found at  $\langle z \rangle = 1.6$ . At  $z < 1$ , conversely, their number density slowly decreases with cosmic time, decoupling from the evolution observed for the general population. At  $z \sim 0$ , the number density of *compact* ETGs has decreased to 16% of the total density (by definition), reaching a value that is, just by chance, comparable to the number density at  $\langle z \rangle = 1.6$  (e.g. Saracco et al. 2010). Similarly, the number density of the *ultra-compact* ETGs drops by a factor of  $\sim 100$  from  $z \sim 1$  to  $z \sim 0$ , and in the local universe ultra-compact ETGs are  $\sim 500$  times rarer than *normal* ETGs. Similar behaviors are exhibited by the mass density in compact ETGs as a function of the redshift in Figure 9.

It is interesting to note that in Figure 8 the number of *normal* early-types from  $z \sim 1$  to  $z \sim 0.5$  increases at a faster rate than the one at which the *compact* ones disappear. As a result, the total number density increases, as already described. This result implies once again that both the mechanisms mentioned at the beginning of this section are at work from  $z \sim 1$  to  $z \sim 0$ . On one side, some of the *compact* galaxies gradually increase in size, moving onto the local relation, and causing number (and mass) density of compact early-types to decrease; the *compact* galaxies that become *normal* support in part the growth of the mass and number density of *normal* early-types; but since the total number (compact+normal) increases as well, it means that new passive galaxies with sizes comparable to local counterparts are formed.

In the bottom panel of Fig. 8 we show the fraction of compact and ultra-compact ETGs as a function of the redshift and cosmic time. The fraction of compact ETGs decreases from 80% at  $\langle z \rangle = 1.6$  to 16% at  $z = 0$ , while the fraction of ultra-compact drops from 40% at  $\langle z \rangle = 1.6$  to zero at  $z = 0$ . We stress that these fraction can be slightly overestimated at  $1.2 < z < 2.5$ , as a result of the incompleteness of our selection at  $z > 1.6$ . Anyway, strong lower limits to these fractions (if we limit the sample to  $1.2 < z < 1.6$ ) are set to 65 and 25%, respectively. We note again that Saracco et al. (2010) found a much smaller fraction of compact early-types at  $z \sim 2$ , and we tried to explain such difference in the previous Section. However, our estimates for the compact fraction are in quite good agreement at later epochs with the measurements by Valentinuzzi et al. (2010a,b). In particular, Valentinuzzi et al. (2010a) analyzed a sample of  $z \sim 0.04$  massive galaxies in clusters (WINGS survey,

Fasano et al. 2006), and found a significant fraction of very compact galaxies. Valentinuzzi et al. (2010b) found a similar rich population of compact galaxies in clusters at  $z \sim 0.7$  (EDisCS, White et al. 2005), and claimed that 17% and 44% of all cluster galaxies are compact in WINGS and EDisCS clusters, respectively. By knowing the fraction of galaxies in the two surveys that are not morphologically early-type, we could reconstruct the fraction of compact early-types that we report in the bottom panel of Fig. 8.

## 6. DISCUSSION AND CONCLUSIONS

In this paper we have analyzed a complete and homogeneous sample of passive galaxies from  $z \sim 0$  to  $z \sim 2.5$ , with the aim of observationally constrain the mass and size evolution of such systems during the last 10 Gyr of cosmic time. In particular, we estimated the evolution of the relative abundance of *compact*, *ultra-compact* and *normal* ETGs throughout this redshift range.

We selected a homogeneous and robust sample of 563 passive galaxies using the multiband photometry available in the GOODS N+S fields, selecting galaxies with  $M > 10^{10} M_{\odot}$  and  $SSFR < 10^{-2} \text{Gyr}^{-1}$ . We studied the morphological properties of the sample in the optical rest-frame, using the ACS  $z$ -band for objects at  $z < 1.2$  and the WFC3  $H$ -band for galaxies at  $z > 1.2$ , and we discarded galaxies with late-type morphologies. We then run GALFIT to measure the Sérsic indices and physical sizes.

We found that, at all redshifts, the morphology traced by the rest-frame UV light is, within the statistical uncertainties, very close to that traced by the optical light, at least when parameters such as the Sérsic indices and effective radii are used. In fact, the sizes and Sérsic indices measured in the UV and optical rest-frame correlate quite well with each other, with the sizes measured in the optical rest-frame being slightly smaller (by  $\sim 20\%$  and  $\sim 10\%$  at  $z \gtrsim 1$  and  $z \lesssim 1$ , respectively) than those derived from the UV rest-frame. This shows that, at least for galaxies that are not currently forming stars, the morphological K-correction is weak, and thus that ACS/ $z$ -band observations, if deep enough, can be indeed used to measure the size of passive galaxies at  $z > 1$ . This is in good agreement with previous results by Trujillo et al. (2007) and Cassata et al. (2010) and, at lower redshift, with Cassata et al. (2005) and Papovich et al. (2003).

We showed that the mass-size relation of ETGs evolves significantly from  $z > 1.6$  to  $z \sim 0$ :  $\sim 80\%$  of ETGs at  $z > 1.6$  in our sample are smaller than local counterparts of the same mass, and at later epochs ETGs are increasingly larger. We showed as well that the fractional increase of the average size is almost independent on the stellar mass.

With the aim of understanding whether the evolution of the mass-size relation is driven by the size growth of each individual galaxy or by the appearance of new large ETGs, we have built the size distribution in four redshift bins, scaled to the number density of ETGs in each bin. We observed that ETGs at  $1.2 < z < 2.5$  are on average 0.5 dex smaller than local counterparts of the same mass, and we identified a rich population of *ultra-compact* ETGs that have no identified counterparts in terms of size and density in the local Universe. As the time goes

by, at  $0.95 < z < 1.2$  the number of ETGs is increased by a factor of 5, and the new ETGs have a broad range of sizes, from 0.5 dex smaller to 0.5 dex larger than local counterparts of the same mass. At  $z < 0.95$  the evolution is milder, with the number of ETGs increasing of another factor of 1.5 down to  $z \sim 0$ ; the sizes of the new ETGs formed in this phase are similar to the average local value; at the same time the small ETGs gradually disappear, growing in size and skewing the size distribution towards large sizes. These results show that both the mechanisms driving the evolution of the mass-size relation are at work at the same time.

We measured the mass and number density of early-type galaxies as a function of redshift, including the evolution of the relative fraction of *normal*, *compact* and *ultra-compact* ones. More in details, we showed that the number and mass density of massive and passive early-types increase by a factor of  $\sim 5$  within the  $\sim 2$  Gyr between  $z \sim 1.6$  to  $z \sim 1$ , in agreement with Arnouts et al. (2007) and Ilbert et al. (2010). In the following 4 Gyr, from  $z \sim 1$  to  $z \sim 0.5$ , the number density increases by at most another factor of  $\sim 1.5$ , while in the same interval the mass density remains constant. This implies that, as expected in a “downsizing” scenario, the added galaxies that drive the number evolution have small masses and do not contribute too much to the mass density. These findings are in good agreement with Franceschini et al. (2006), Borch et al. (2006) and Abraham et al. (2007), and similar to the results by Cimatti, Daddi & Renzini (2006) and Scarlata et al. (2007).

From  $z \sim 1$  to  $z \sim 0$ , we showed also that the number (and mass) density of *compact* early-types decreases by a factor of 2, while the number density of normal-size ETGs increases much faster, indicating once again that the overall increase of the average size at fixed mass is only partly due to a size increase of individual galaxies, whereas part of the effect is due to the appearance of new ETGs with large size.

We interpret these results as the evidence that the phases at  $z > 1$  and  $z < 1$  are dominated by distinct and different physical mechanisms. The scenario that comes out is the following: the epoch at  $1 < z < 3$  is when the bulk of the stellar mass in local early-type galaxies is assembled. This process of assembly is quite rapid: the stellar mass locked in passive early-type galaxies increases by a factor of 5 over a period of  $\sim 2$  Gyr. Whatever the mechanism responsible for this huge mass density increase (gas-rich major merger, collapse of unstable disks, monolithic collapse), it produces a remnant that is compact and small with respect to local counterparts:  $\sim 80\%$  of early-types in this redshift interval are smaller than galaxies of the same mass in the local Universe. Interestingly, Targett et al. (2011) found that submillimeter galaxies at  $z \sim 2$  have similar sizes to those that we measure for ETGs at the same epoch, suggesting a possible evolutionary connection between the two classes of galaxies. On the other hand the evolution at  $z < 1$  is much milder. In this phase, the compact galaxies continuously increase in size, eventually disappearing, most likely undergoing a series of dry and wet minor mergers or by slowly accreting a small amount of mass in their outskirts (e.g. Van Dokkum et al. 2010; Hopkins et al. 2009). At the same time, new ETGs are

formed, driving the number density increase of a factor 1.5 that we observe from  $z \sim 1$  to  $z \sim 0$ . These new ETGs have small masses and large sizes, indicating that the mechanism through which they are formed is different from the one that at  $z > 1$  generated the compact ETGs.

PC, MG, YG and SS acknowledge support from NASA grants HST-GO-9425.36-A, HST-GO-9822.45-A, and HST-GO-10189.15-A, awarded by the Space Telescope Science Institute, which is operated by the Asso-

ciation of Universities for Research in Astronomy, Inc. (AURA) under NASA contract NAS 5-26555. The work presented here is partly based on observations obtained with WIRC*am*, a joint project of Canada-France-Hawaii Telescope (CFHT), Taiwan, Korea, Canada, France, at the CFHT which is operated by the National Research Council (NRC) of Canada, the Institut National des Sciences de l'Univers of the Centre National de la Recherche Scientifique of France, and the University of Hawaii. We are grateful to the anonymous referee for the useful comments.

## REFERENCES

- Abraham, R. G., Nair, P., McCarthy, P. J., et al. 2007, *ApJ*, 669, 184
- Arnouts, S., Walcher, C. J., Le Fèvre, O., et al. 2007, *A&A*, 476, 137
- Beckwith, S. V. W., Stiavelli, M., Koekemoer, A. M., et al. 2006, *AJ*, 132, 1729
- Bell, E. F., McIntosh, D. H., Katz, N., et al. 2003, *ApJS*, 149, 289
- Blanton, M. R., Schlegel, D. J., Strauss, M. A., et al. 2005, *AJ*, 129, 2562
- Borch, A., Meisenheimer, K., Bell, E. F., et al. 2006, *A&A*, 453, 869
- Bruzual, G., & Charlot, S., 2003, *MNRAS*, 344, 1000
- Brinchmann, J., Charlot, S., White, S. D. M., et al. 2004, *MNRAS*, 351, 1151
- Buitrago, F., Trujillo, I., Conselice, C. J., et al. 2008, *ApJ*, 687, L61
- Calzetti, D., Armus, L., Bohlin, R. C., et al. 2000, *ApJ*, 533, 682
- Cassata, P., Cimatti, A., Franceschini, A., et al. 2005, *A&A*, 357, 903
- Cassata, P., Cimatti, A., Kurk, J., et al. 2008, *A&A*, 3, 39L
- Cassata, P., Giavalisco, M., Guo, Yicheng, et al. 2010, *ApJ*, 714, L79
- Cimatti, A., Daddi, E., & Renzini, A., 2006, *A&A*, 453, 29
- Cimatti, A., Cassata, P., Pozzetti, L., et al. 2008, *A&A*, 482, 21
- Conselice, C., Bluck, A. F. L., Buitrago, G., et al. 2011, accepted for publication in *MNRAS*
- Daddi, E., Renzini, A., Pirzkal, N., et al. 2005, *ApJ*, 626, 680
- Fasano, G., Marmo, C., Varela, J., et al. 2006, *A&A*, 445, 805
- Fioc, M., & Rocca-Volmerange, B., 1997, *A&A*, 326, 950
- Fontana, A., Salimbeni, S., Grazian, A., et al. 2006, *A&A*, 459, 745
- Förster-Schreiber, N. M., Genzel, R., Lehnert, M. D., et al., 2006, 645, 1062
- Förster-Schreiber, N. M., Genzel, R., Bouché, N., et al., 2009, 706, 1364
- Franceschini, A., Rodighiero, G., Cassata, P., et al. 2006, *A&A*, 453, 397
- Genzel, R., Burkert, A., Bouché, N., et al., 2008, *ApJ*, 687, 59
- Giavalisco, M., Dickinson, M., Ferguson, H. C., et al. 2004, *ApJ*, 600, 103
- Guo, Yicheng, et al., 2011a, in prep.
- Guo, Yicheng, Giavalisco, M., Cassata, P., et al., 2011b, *ApJ*, 735, 18
- Hopkins, P. F., Bundy, K., Murray, N., et al., 2009, *MNRAS*, 398, 898
- Ilbert, O., Salvato, M., Le Floc'h, E., et al., 2010, *ApJ*, 709, 644
- Laidler, V. G., Papovich, C., Grogan, N. A., et al., 2007, *PASP*, 119, 1325
- Kauffmann, G., Heckman, T. M.; White, S. D. M., et al., 2003, *MNRAS*, 341, 33
- Khochfar, S., & Silk, J., 2006, *ApJ*, 648, L21
- Koekemoer, A. M., et al., 2002, HST Calibration Workshop (eds. S. Arribas, A. M. Koekemoer, B. Whitmore, Baltimore: STScI), 337
- Koekemoer, A. M., Faber, S. M., Ferguson, H. C., et al., 2011, *ApJS*, [astro-ph/1105.3754]
- Mancini, C., Daddi, E., Renzini, A., et al. 2010, *MNRAS*, 401, 933
- Maraston, C., Pforr, J., Renzini, A., et al. 2010, *MNRAS*, 407, 830
- Marchesini, D., Van Dokkum, P. G., Förster-Schreiber, N. M., 2009, et al., *ApJ*, 701, 1765
- McCarthy, P. J., Yan, H., Abraham, R. G., et al. 2007, *ApJ*, 664, 17
- Nonino, M., Dickinson, M., Rosati, P., et al. 2009, *ApJS*, 183, 244
- Naab, T., Johansson, P. H., & Ostriker, J. P., 2009, *ApJ*, 699, 178L
- Papovich, C., Giavalisco, M., Dickinson, M., et al. 2003, *ApJ*, 598, 827
- Peng, Y., Lilly, Simon J., Kovac, K., et al. 2010, *ApJ*, 721, 193
- Peng, C. Y., Ho, Luis C., Impey, C. D., et al. 2002, *AJ*, 124, 266
- Popesso, P., Dickinson, M., Nonino, M., et al. 2009, *A&A*, 494, 443
- Ryan, R. E. Jr., McCarthy, P. J., Cohen, S. H., et al. 2011, submitted to *ApJ*, [astro-ph/1007.1460]
- Ravindranath, S., Giavalisco, M., Ferguson, H. C., et al. 2006, *ApJ*, 652, 963
- Salimbeni, S., Fontana, A., Giallongo, E., et al., 2009, in AIP Conf. Proc. 1111, Probing Stellar Populations Out to the Distant Universe, ed. G. Giobbi et al. (Melville, NY: AIP), 207
- Salpeter, E. E., 1955, *ApJ*, 121, 161
- Saracco, P., Longhetti, M., & Andreon, S., et al. 2009, *MNRAS*, 392, 718
- Saracco, P., Longhetti, M., Gargiulo, A., et al. 2010, *MNRAS*, 408, 21
- Scarlata, C., Carollo, C. M., Lilly, S. J., et al. 2006, *ApJS*, 172, 494
- Shankar, F., Marulli, F., Bernardi, M., et al. 2010, *MNRAS*, 405, 948
- Shankar, F., Marulli, F., Bernardi, M., et al. 2011, submitted to *MNRAS*, [astro-ph/1105.6043]
- Shen, S., Mo, H. J., White, S. D. M., et al. 2003, *MNRAS*, 343, 978
- Shih, H., & Stockton, A., 2011, *ApJ*, 733, 45
- Somerville, R. S., Hopkins, P. F., Cox, T. J., et al. 2008, *MNRAS*, 391, 481
- Stott, J. P., Collins, C. A., Burke, C., et al. 2011, *MNRAS*, 414, 445
- Szomoru, D., Franx, M., van Dokkum, P. G., et al. 2010, *ApJ*, 714, 244
- Targett, T. A., Dunlop, J. S., McLure, R., et al. 2010, *MNRAS*, 412, 295
- Taylor, E. N., Franx, M., Glazebrook, K., et al. 2010, *ApJ*, 720, 723
- Thomas, D., Maraston, C., Schawinski, K., et al. 2010, *MNRAS*, 404, 1775
- Toft, S., van Dokkum, P., Franx, M., et al. 2007, *ApJ*, 671, 285
- Trujillo, I., Conselice, C. J., Bundy, K., et al. 2007, *MNRAS*, 382, 109
- Trujillo, I., Cenarro, A. J., de Lorenzo-Caceres, A., et al. 2009, *ApJ*, 692, 118
- Van Dokkum, P. G., Franx, M., Kriek, M., et al. 2008, *ApJ*, 677, L5
- Van Dokkum, P. G., Whitaker, K. E., Brammer, G., et al. 2010, *ApJ*, 709, 1018
- Valentinuzzi, T., Fritz, J., Poggianti, B. M., et al. 2010a, *ApJ*, 712, 226
- Valentinuzzi, T., Poggianti, B. M., Saglia, R. P., et al. 2010b, *ApJ*, 721, L19
- van der Wel, A., Bell, E. F., van den Bosch, F. C., et al. 2009, *ApJ*, 698, 1232
- Vanzella, E., Cristiani, S., Dickinson, M., et al. 2008, *A&A*, 478, 83

- ang, W. H., Cowie, L. L., Barger, A., et al., 2010, ApJS, 187, 251
- White, S. D. M., Clowe, D. I., Simard, L., et al. 2005, A&A, 444, 365
- Windhorst, R. A., Cohen, S. H., Hathi, N. P., et al. 2011, ApJS, 193, 27
- Zirm, A. W., van der Wel, A., Franx, M., et al. 2007, ApJ, 656, 66